A R C H I V E S O F M E T A L L U R G Y A N D M A T E R I A L S
Volume 60 2015 Issue 2
DOI: 10.1515/amm-2015-0093

G.-G. LEE*,♯, H.-H. JIN*, K. CHANG*, B.H. LEE**, J. KWON*

ATOMISTIC ANALYSIS OF RADIATION-INDUCED SEGREGATION IN ION-IRRADIATED STAINLESS STEEL 316

ANALIZA W SKALI ATOMOWEJ INDUKOWANEJ PROMIENIOWANIEM SEGREGACJI W STALI NIERDZEWNEJ 316

Stainless steel (SS) is a well-known material for the internal parts of nuclear power plants. It is known that these alloys exhibit radiation-induced segregation (RIS) at point defect sinks at moderate temperature, while in service. The RIS behavior of SS can be a potential problem by increasing the susceptibility to irradiation-assisted stress corrosion cracking. In this work, the RIS behavior of solute atoms at sinks in SS 316 irradiated with Fe^{4+} ions were characterized by atom probe tomography (APT). There were torus-shaped defects along with a depletion of Cr and enrichment of Ni and Si. These clusters are believed to be dislocation loops resulting from irradiation. The segregation of solutes was also observed for various defect shapes. These observations are consistent with other APT results from the literature. The composition of the clusters was analyzed quantitatively almost at the atomic scale. Despite the limitations of the experiments, the APT analysis was well suited for discovering the structure of irradiation defects and performing a quantitative analysis of RIS in irradiated specimens.

Keywords: atom probe tomography (APT), radiation-induced segregation (RIS), ion irradiation, irradiation defects, stainless steel

1. Introduction

Irradiation of energetic particles onto a structural material produces various kinds of defects. Among such irradiation defects, vacancies and self-interstitial atoms can diffuse and may be reincorporated into the crystal structure at defect sinks, such as surfaces, grain boundaries, and dislocations. These additional defect fluxes induce diffusion of the solute atoms and, consequently, the preferential interaction of the solute atoms with mobile defects results in the enrichment or depletion of the solutes at the defect sinks. These phenomena are generally known as radiation-induced segregation (RIS) [1].

Austenitic stainless steel (SS) is widely used for reactor internal parts in nuclear power plants. Neutron irradiation leads to RIS in SS during service–corresponding to the depletion of Cr and the enrichment of Ni, Si, and P at defect sinks. The depletion of Cr might enhance irradiation-assisted stress corrosion cracking of SS, and this might reduce the integrity of nuclear power plants, especially in case of boiling water reactors [2-3]. Thus, numerous studies on RIS in SS and model alloys have been performed over the three last decades [4-13].

To obtain a concentration profile of RIS arising from irradiation, scanning transmission electron microscopy (STEM) and energy dispersive X-ray spectroscopy (EDS) are generally used as basic analysis techniques. However, the resolution of EDS is limited by the beam size, which is rarely better than 2 nm due to beam broadening, and the actual peak concentration of RIS may be underestimated in EDS [14]. Furthermore, in case of analyzing RIS around irradiation defects in a matrix, the overlapping of the probed volume with the matrix prohibits a quantitative analysis of concentration changes.

In the current work, we introduced atom probe tomography (APT) to analyze RIS in SS 316. APT has many merits for the analysis of small precipitates in a material [15,16]. The various types of radiation-induced defects were identified and the compositional characteristics were quantitatively provided with a wide view point. The measured concentrations were compared with values of the literature [17,18]. To estimate the RIS behavior, a basic modeling was established and compared with the literature. This work can provide a fundamental understanding of the RIS behavior in ion-irradiated SS 316.

2. Experimental

The test sample was taken from a solution-annealed plate made of SS 316. The chemical composition of the plate is given in Table 1. The most important solutes for RIS were Cr, Ni, and Si. A small plate of $10\times10\times2.5$ mm^3 was prepared for the ion irradiation test. The specimen was ground with 1200 mesh SiC paper, and finally polished with a paste of 0.25-μm diamond suspension.

Ion irradiation was carried out using a tandem ion accelerator at the Korean Institute of Geoscience and Mineral Re-

* KOREA ATOMIC ENERGY RESEARCH INSTITUTE (KAERI), DAEJEON, KOREA
** DAEGU GYEONGBUK INSTITUTE FOR SCIENCE AND TECHNOLOGY (DGIST), DAEGU, KOREA
♯ Corresponding author: gglee@kaeri.re.kr

sources. The ion source was Fe^{4+}, and the acceleration voltage was 2 MeV. The temperature of the specimen was maintained at ~400°C. The total ion fluence and irradiation time were 5.6 $\times 10^{15}$ ions/cm^2 and 4 h, respectively. The peak dose of the irradiation was estimated to be 12 dpa at a depth of 1.7 μm by using the SRIM code with the full cascade evaluation mode [19]. Considering the ion irradiation and accumulation effect, the region at a depth of 1 μm below the irradiated surface was selected for the APT analysis. The dose of the specimen was estimated to be about 4 dpa. Fig. 1 shows the irradiation damage and accumulated Fe ion concentration as a function of the depth on the basis of SRIM calculations.

TABLE 1
Composition of stainless steel 316 in weight and atomic percentages

	Cr	Ni	Si	Mo	Mn	P	C	S	Fe
wt%	16.7	11.1	0.59	2.0	1.3	0.05	0.047	0.001	balance
at%	17.8	10.5	1.17	1.2	1.3	0.09	0.217	0.002	balance

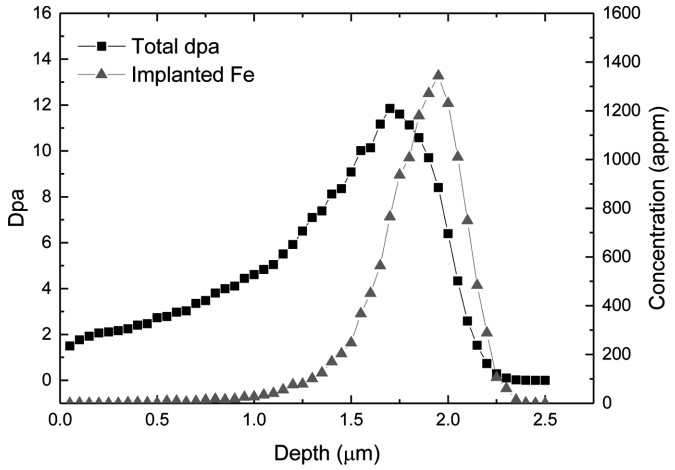

Fig. 1. Irradiation dose and concentration of Fe^{4+} ions as a function of the depth, estimated by SRIM

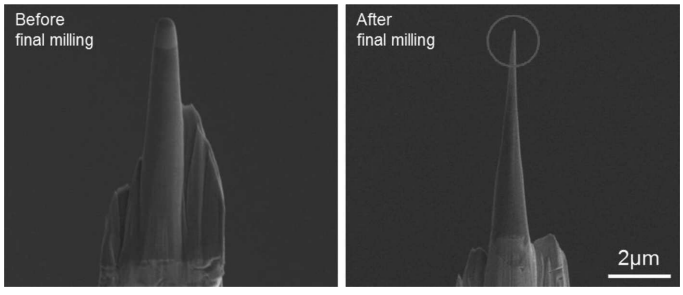

Fig. 2. Micrographs of an APT specimen prepared using the focused ion beam technique

Atom probe needles were prepared using a Helios Nanolab 650 dual beam SEM/FIB instrument from FEI. The detailed procedure of the preparation of APT is described elsewhere [17]. Fig. 2 shows an APT needle micromachined by means of the focused ion-beam (FIB) technique. APT measurements were carried out using a laser-assisted, wide angle atom probe from CAMECA. The analysis was carried out at 30 K using 500 fs laser pulses in the UV region at 343 nm and at a 100-kHz repetition rate. The evaporation rate was 0.002-0.050 per laser pulse, and the applied laser power was 15000 μW. The corresponding element-specific atomic positions within the 3D volume were reconstructed using the Tap3Ddata program from CAMECA, and complemented by the analysis program developed at the Korea Atomic Energy Research Institute.

3. Results and discussion

Fig. 3 shows a cross-sectional view of the irradiated sample. A grain boundary was located between two grains. A damaged region parallel to the surface was observed at about 2 μm in depth below the surface. The SRIM calculation expected the peak-damaged region and the implanted region to be located at about 1.7 μm and 2.0 μm, respectively. The experimental observation shows good agreement with the calculation. To check the RIS behavior of the specimen, the grain boundary region at 1 μm in depth was cut, and the compositional change of the specimen was analyzed using TEM/EDS. A typical RIS behavior was observed, namely depletion of Cr and enrichment of Ni. The concentration of Cr decreased from 16.7 wt% to 13.9 wt%, and the peak concentration of Ni increased from 11.1 wt% to 15.3 wt%.

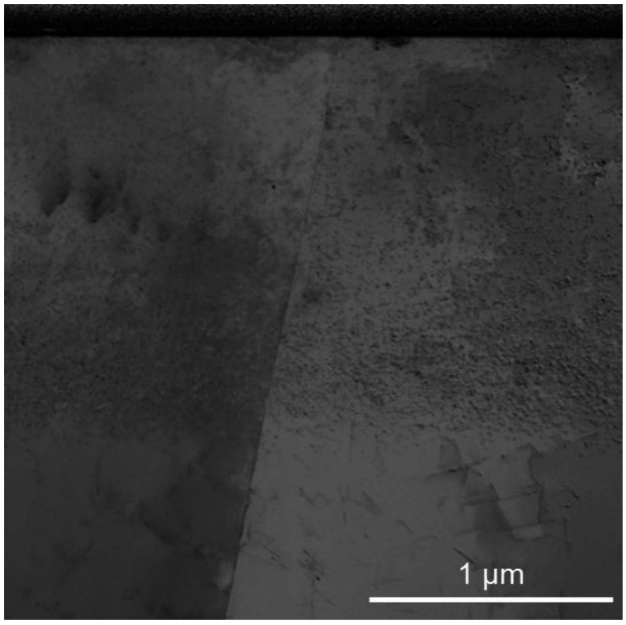

Fig. 3. Cross-sectional micrograph of the irradiated sample

There are irradiation defects in the matrix region of the sample. Fig. 4 shows a TEM micrograph of the damaged matrix region located at the depth of 1 μm below the surface. Dislocation loops and black disks are clearly observed. The loop size is measured to be 20-30 nm, and the loops are arranged along special orientations. By such TEM observations, the shape and density of the irradiation defects are easily characterized, but compositional changes at the irradiation defects cannot be measured quantitatively because the loops are located in the matrix and it is hard to distinguish the defect concentration from the matrix concentration. This is why APT has been performed additionally. APT can provide the quantitative concentrations of the elements at irradiation defects in the matrix.

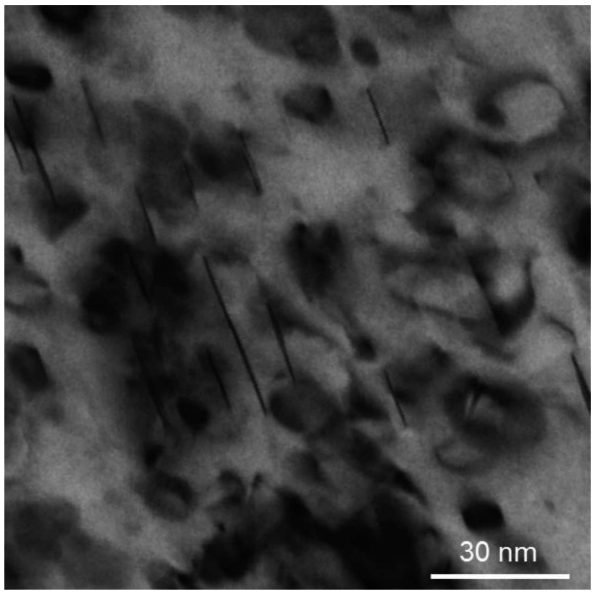

Fig. 4. TEM micrograph of the damaged matrix region at 1 μm in depth from the surface

Fig. 5 shows atomic maps of the elements in the APT specimen. The volume of the needle was measured to be 114×115×205 nm^3, and about 10 million atoms were collected and reconstructed. Because of the large number of atoms, the enrichment of Ni and depletion of Cr were not evident in Fig. 5. Additionally, it is not easy to identify depletion or enrichment of Mn, P, and C at irradiation defects. In contrast, Si is enriched clearly at the irradiation defects. To obtain a detailed view of the Si enrichment, the atomic map of Si was rotated and various forms of Si enrichment were found, specifically torus-shaped, disk-shaped, and rounded clusters, as well as 1D, linear features. The torus-shaped and disk-shaped clusters are similar to the TEM observation presented in Fig. 4. The APT analysis enabled us to easily capture a 3D configuration of irradiation defects. An additional quantitative analysis of the elemental concentrations at the irradiation defects was carried out.

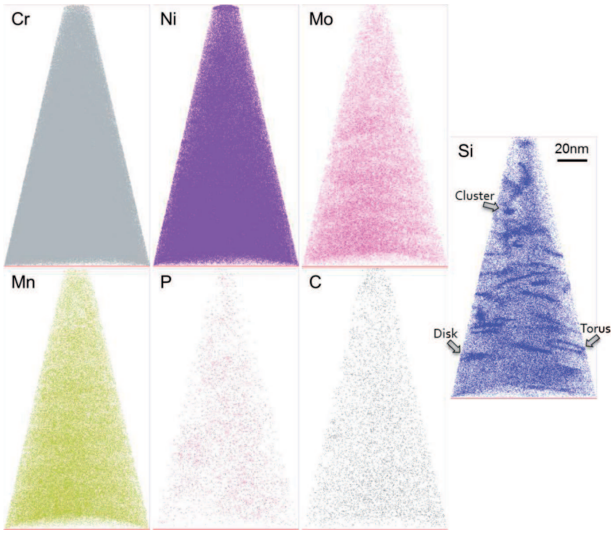

Fig. 5. Atomic maps of various solutes in ion-irradiated SS 316. The Si map clearly shows enrichments at various irradiation defects. Arrows with defect descriptions indicate the positions of the local quantitative analyses

Fig. 6 shows the analysis of a torus-shaped cluster in the APT specimen. The cylindrical region around the target was cut from the total atomic map, and the relative concentrations of Si, Ni, and Cr are shown in the corresponding 2D plots. The quantitative concentration along the red line of the selected volume was determined and is also presented in Fig. 6. The cluster is supposed to be a dislocation loop enriched with Ni and Si atoms. As shown in Fig. 6, Si atoms are located mostly at the edge of the dislocation loop, whereas the center of the loop shows a reduced concentration of Si. This means that Si is closely correlated with the core structure of the dislocation loop. The peak concentration of Si reached about 25 at%

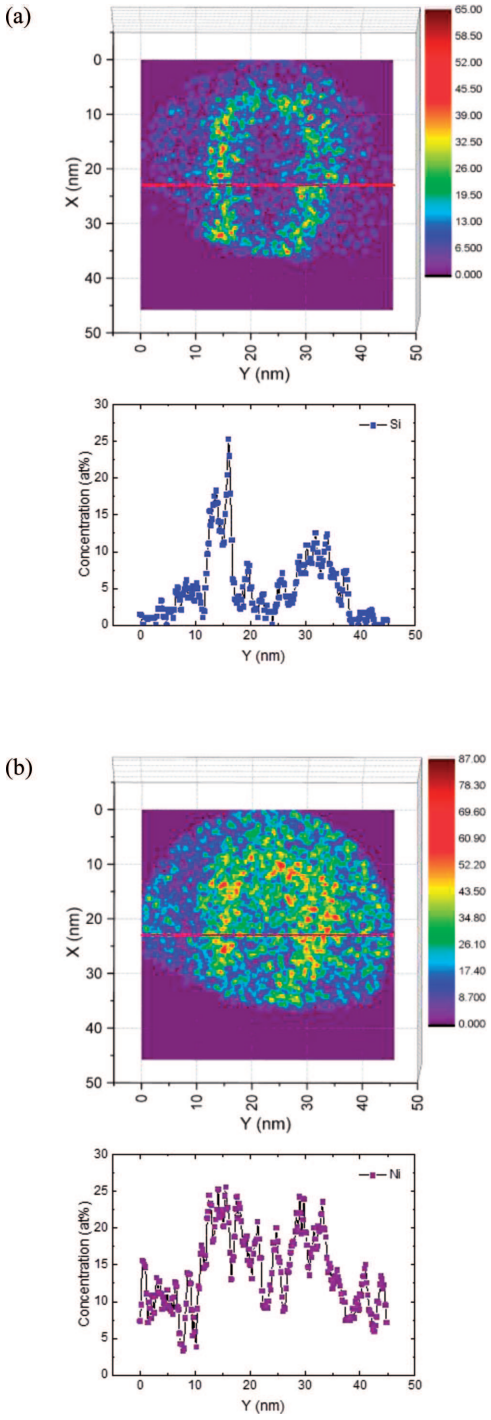

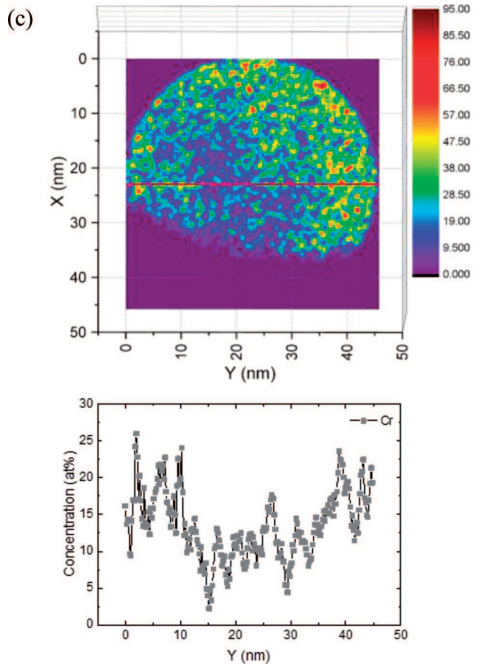

Fig. 6. Concentration profiles of (a) Si, (b) Ni, and (c) Cr in the torus-shaped dislocation loop. The 2D color maps show the relative concentrations which were obatined from a cylindrical region with diameter and thickness of d = 46 nm and t = 9.2nm, respectively. The corresponding 1D concentration profiles are plotted for binned sections of 4×4 nm^2 and 0.2 nm step width along the red central line

(starting from 1 at%). Also Ni atoms are enriched in the dislocation loop, however, with a much more gradual distribution compared with Si. Basically, Ni is a substitutional solute atom in SS 316, and the basic RIS mechanism of Ni is known as the inverse Kirkendall effect (vacancy migration mechanism). On the other hand, the Si concentration is believed to be more strongly correlated to interstitial atoms. The peak concentration of Ni reached about 25 at%, starting from 9.3 at%. The depletion of Cr was also observed in the dislocation loop. The Cr concentration profile slightly deviated around the edge of the loop, compared to the Ni concentration. The minimum concentration of Cr reached about 2.2 at%. It is apparent that APT has high resolution of quantitatively analysis.

Fig. 7 shows the results of the compositional analysis of the rounded cluster. The concentrations of Si and Ni are strongly localized and enriched at the center of the defect. The peak concentrations of Si and Ni reached about 28 at% and 26 at%, respectively. From these results, Ni_3Si precipitate is supposed to be formed during irradiation. However, the atomic ratio between Ni and Si was larger than 3 and the structure of Ni_3Si was not confirmed by APT. Thus, further analysis technique is needed to reveal the nature of the cluster in detail.

Table 2 summarizes the compositions of the irradiation defects of the present work and previously reported APT results of SS irradiated under various conditions [17,18]. In our present study, Si and Ni are highly enriched, and the dislocation loop and the rounded cluster show a very high peak concentration of Si. Although the quantitative concentration of the APT specimen is closely related to the binning size of atoms in the selected region of the atomic maps, the distinct enrichment of Si was clearly evident. The results of Etienne on cold-worked SS316, irradiated with Fe^{5+} ions at 350°C to 10 dpa, showed similar defect types: torus-shaped and rounded Ni-Si clusters, and segregation at dislocations and grain boundaries [17]. The rounded clusters showed the highest enrichment of Si, similar to our present results. On the other hand, the results of Toyama on SS304, irradiated with neutrons at 300°C to a dose of 24 dpa, showed only two types of irradiation defects, namely rounded clusters and grain boundaries [18]. The clusters showed high enrichments of Si and Ni, while the grain boundaries showed modest RIS behavior. It is important that the irradiation conditions affected the defect types, defect sizes, and concentrations of the solutes. Among the various defect types, rounded clusters showed very high enrichment/depletion of solutes.

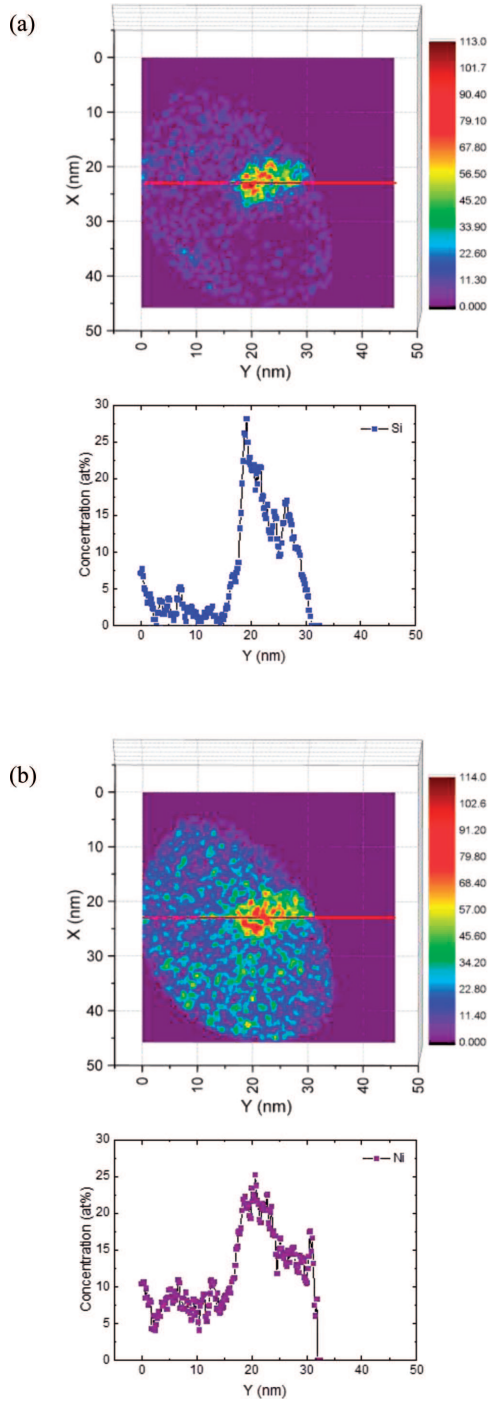

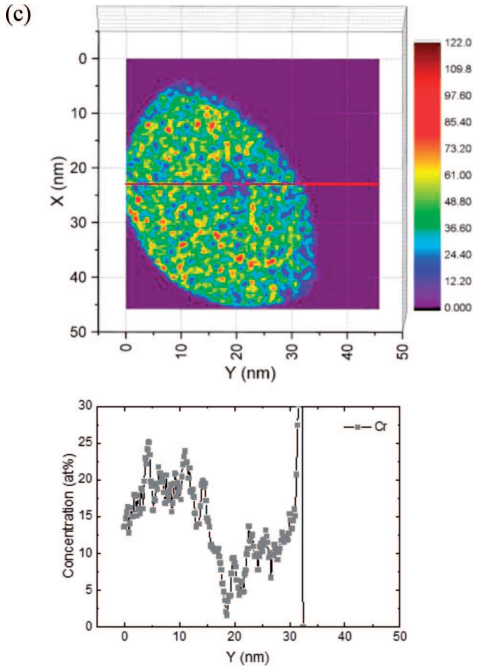

Fig. 7. Concentration profiles of (a) Si, (b) Ni, and (c) Cr in the rounded cluster. The 2D color maps show the relative concentrations which were obatined from a cylindrical region with diameter d = 46 nm and thickness t = 9.2nm). The corresponding 1D concentration profiles are plotted for binned sections of 4×4 nm^2 and 0.2 nm step width along the red central line

TABLE 2
Compositions of the selected irradiation defects

		Si	Ni	Cr	Note
This work	Cluster	28.2	25.2	1.6	Peak
	Torus	25.3	25.6	2.2	Peak
Etienne [17]	Cluster	12.3	28.2	10.2	Average
	Torus	7.6	25.6	10.7	Average
	GB	6.32 (8.7)	26.6 (19.9)	9.4 (7.4)	Average
Toyama [18]	Cluster	14	40	11	Average
	GB	6.8 (8.5)	19 (20.3)	14 (7.4)	Peak

*Values in parenthesis are estimated by the modeling of this work

The RIS behavior at grain boundaries can be described by the well-established Fe-Cr-Ni modeling of Perks [20]. We have already applied this type of modeling to RIS in SS 316, and the detailed methodology is described in our previous work [21]. To calculate the Si concentration, we extended the model by additionally considering the solute-interstitial correlation, which was proposed by other researchers [22,23]. The material parameters for the model were given in our previous work [21]. The Si-related factors are given in Table 3. The estimated peak concentrations at the grain boundaries are given in parentheses in Table 2. The Ni enrichment was underestimated under the conditions of Etienne, and the Cr depletion was slightly overestimated under the conditions of Toyama. The estimation of the Si enrichment was rather acceptable in both cases. Note that loops and rounded clusters were not estimated. The RIS of the loops and clusters showed very high enrichment/depletion behavior. Thus, future work for advanced modeling is needed.

TABLE 3
Model parameters accounting for the Si-intestinal correlation

Parameter	Symbol	Value
Relative vacancy jump rate for Si	ω_{Si}	1.0
Si-vacancy correlation factor	f_v^{Si}	4.38
Relative interstitial jump rate for Si	ω_{Si-i}	0.4
Si-interstitial binding energy	E_b^{Si-i}	0.17 eV

In our results, there are some limitations. We did not find a grain boundary in our APT specimen and, thus, it was impossible to compare the APT with the TEM/EDS results. In addition, APT has a rather low atomic yield, and many unidentified atoms are present in our results at the level of about ~20%. This may affect the accuracy of the quantitative analysis of APT. However, this limitation will be overcome by the improvement of the APT analyzer in the future.

4. Conclusions

In this study, APT analysis of RIS in ion-irradiated SS316 was performed. Various types of irradiation defects were observed. Si atoms are predominantly located at the core structures of dislocation loops and clusters. The RIS in irradiation defects was more pronounced compared to the RIS in grain boundaries, as inferred from the literature. It is believed that there were strong Si-interstitial interactions during irradiation. The 1D modeling of RIS in SS 316 was implemented, and the peak concentration at grain boundaries was reproduced fairly. Despite the limitations of the experiments and modeling, the APT analysis was well suited for discovering the structure of irradiation defects and the quantitative analysis of RIS in irradiated specimens.

Acknowledgements

This work was supported by the National Research Foundation of Korea (NRF) grant funded by the Korean government (MSIP). [2012M2A8A4025886].

REFERENCES

[1] G.S. Was, Fundamentals of Radiation Materials Science, Springer, New York, 2007.
[2] P. Scott, J. Nucl. Mater. **211**, 101 (1994).
[3] S.M. Bruemmer, E.P. Simonen, P.M. Scott, P.L. Andresen, G.S. Was, J.L. Nelson, J. Nucl. Mater. **274**, 299 (1999).
[4] R.A. Johnson, N.Q. Lam, Phys. Rev. B. **13**, 4364 (1976).
[5] P.R. Okamoto, L.E. Rehn, J. Nucl. Mater. **83**, 2 (1979).
[6] A.D. Marwick, R.C. Piller, P.M. Sivell, J. Nucl. Mater. **83**, 35 (1979).
[7] T.R. Allen, J.T. Busby, G.S. Was, J. Nucl. Mater. **255**, 44 (1998).
[8] T.R. Allen, G.S. Was, Acta Mater. **46**, 3679 (1998).
[9] T.S. Duh, J.J. Kai, F.R. Chen, L.H. Wang, J. Nucl. Mater. **294**, 267 (2001).
[10] J.J. Kai, F.R. Chen, T.S. Duh, Mater. Trans. **45**, 40 (2004).

[11] N. Sakaguchi, H. Takahashi, H. Ichinose, Mater. Trans. **46**, 440 (2005).
[12] K.G. Field, L.M. Barnard, C.M. Parish, J.T. Busby, D. Morgan, T.R. Allen, J. Nucl. Mater. **435**, 172 (2013).
[13] R. Hu, G.D.W. Smith, E.A. Marquis, Acta Mater. **61**, 3490 (2013).
[14] K. Nakata, O. Okada, Y. Ueki, T. Kamino, J. Electron Microsc. **47**, 193 (1995).
[15] P.-P. Choi, I. Povstugar, J. Kor. Powd. Met. Inst. **19**, 67 (2012).
[16] J.H. Lee, J.H. Kim, J. Kor. Powd. Met. Inst. **20**, 228 (2013).
[17] A. Etienne, B. Radiguet, N.J. Cunningham, G.R. Odette, P. Pareige, J. Nucl. Mater. **406**, 244 (2010).
[18] T. Toyama, Y. Nozawa, W. Van Renterghem, Y. Matsukawa, M. Hatakeyama, Y. Nagai, A. Al Mazouzi, S. Van Dyck, J. Nucl. Mater. **425**, 71 (2012).
[19] J.F. Ziegler, J.P. Biersack, U. Littmark, The Stopping and Range of Ions in Solids, Pergamon, New York, 1985.
[20] J.M. Perks, A.D. Marwick, C.A. English, A computer code to calculate radiation-induced segregation in concentrated ternary alloys, AERE R 12121, 1986.
[21] G.-G. Lee, H.-H. Jin, Y.-B. Lee, J. Kwon, J. Nucl. Mater. **449**, 234 (2014).
[22] H. Wiedersich, P.R. Okamoto, N.Q. Lam, J. Nucl. Mater. **83**, 98 (1979).
[23] K. Fukuya, K. Fujii, J. Nucl. Sci. Technol. **46**, 744 (2009).

Received: 20 November 2014.